Article

Discovery Medicine 2026; 38(210): 2067–2076
https://doi.org/10.24976/Discov.Med.202638210.161

TLR4/NF-κB Signaling Modulates Autophagy and Contributes to Uremic Cardiomyopathy Progression

Huiping Zhu[1], Weinan Wu[1], Liutong Pan[1], Zaiyou Dai[1], Shasha Cai[1,*]

[1]Department of Nephrology, The First People's Hospital of Wenling, 317500 Taizhou, Zhejiang, China
*Correspondence: cassiopeia20230625@163.com (Shasha Cai)
Submitted: 22 May 2026 Revised: 16 June 2026 Accepted: 6 July 2026 Published: 23 July 2026

Background: Uremic cardiomyopathy (UCM) is a severe and irreversible cardiovascular complication that commonly occurs in patients with end-stage renal disease and is associated with poor prognosis. Both toll-like receptor 4 (TLR4)/nuclear factor kappa-B (NF-κB) inflammatory signaling and autophagy dysregulation are critically implicated in the pathogenesis of UCM; however, their internal interactive regulatory network has not been fully clarified. This study was designed to explore the role of TLR4/NF-κB axis in regulating myocardial autophagy and pathological injury in UCM.

Methods: Based on 24 Sprague-Dawley rats, control (sham operation), UCM (5/6 nephrectomy), UCM+Resatorvid (TAK-242, TLR4 inhibitor, 2 mg/kg/day s.c.), and UCM+JSH23 (NF-κB inhibitor, 3 mg/kg/day s.c.) groups were constructed (n = 6/group). Following 10 weeks of observation, renal function, systemic inflammation, cardiac performance, myocardial histopathology, TLR4/myeloid differentiation factor 88 (MyD88) pathway and autophagy-related protein expression were systematically evaluated.

Results: UCM model rats exhibited significant renal function impairment, elevated systemic inflammation, deteriorated cardiac function, as well as severe myocardial hypertrophy, interstitial fibrosis, and increased cardiomyocyte apoptosis ($p < 0.05$). These pathological changes were accompanied by excessive activation of the TLR4/MyD88/p-P65 signaling cascade and obvious changes in autophagy-related molecular expression, as evidenced by an elevated Microtubule-associated protein light chain 3 II (LC3II)/LC3I ratio and higher Beclin 1 levels ($p < 0.001$). Both TAK-242 and JSH23 treatment effectively ameliorated renal and cardiac dysfunction, suppressed adverse myocardial pathological remodeling, and reversed autophagy-related protein expression in UCM rats ($p < 0.05$).

Conclusions: The TLR4/NF-κB signaling axis may contribute to UCM progression via modulating the expression of autophagy-associated proteins. Concurrent inhibition of this axis was correlated with alleviation of renal injury, inflammation and myocardial damage, indicating a potential therapeutic strategy for UCM.

Keywords: UCM; toll-like receptor 4; NF-κB; autophagy; renal injury

Introduction

Chronic kidney disease (CKD) is a prevalent chronic disease worldwide. Approximately 50% of the deaths related to its complications are caused by damage to the cardiovascular system [1]. Even for early-stage CKD patients, the risk of cardiovascular death is much higher than that of disease progression to end-stage renal disease [1,2]. Progressive deterioration of renal function leads to the accumulation of metabolic waste products, forming a "uremic microenvironment" where toxic substances and inflammatory factors interact to induce uremic cardiomyopathy (UCM) [3,4]. UCM is primarily characterized by myocardial hypertrophy, interstitial fibrosis, apoptosis of myocardial cells, and progressive decline in cardiac function [5,6,7]. Current knowledge regarding UCM etiology remains incomplete, and no targeted therapeutic drugs are available in clinical practice.

Innate immune dysregulation plays a pivotal role in UCM pathology. Toll-like receptor 4 (TLR4), a key recognition molecule of the innate immune system, serves as a hub connecting uremic metabolic disorders with myocardial inflammatory injury [8,9]. TLR4 is widely distributed on the surface of cardiomyocytes, vascular endothelial cells and immune cells [10,11]. Previous studies have demonstrated that TLR4 can activate the NOD-like receptor family pyrin domain-containing protein 3 (NLRP3) inflammasome to trigger an inflammatory cascade, and also sense metabolic stress signals in myocardial tissue and convert them into cell damage signals, participating in myocardial remodeling [8]. However, the specific downstream signaling pathways and molecular mechanisms by which it regulates cardiomyocyte function in UCM still need to be systematically analyzed.

Autophagy is an important cellular metabolic process to maintain intracellular homeostasis by eliminating dam-

aged organelles and abnormal proteins, thereby promoting cell survival. Dysregulation of autophagy is closely related to the development of cardiomyopathy [12,13]. Under physiological conditions, moderate autophagy has a protective effect on cardiomyocytes, while excessive autophagy activation in pathological conditions such as UCM disrupts metabolic balance, accelerates cardiomyocyte apoptosis and functional failure, and promotes disease progression [14]. TLR4 is closely linked to the regulation of autophagy, and its activation can regulate the expression of autophagy-related genes via transcription factors (e.g., nuclear factor kappa-B (NF-κB)), thereby regulating autophagy levels [15,16]. However, whether NF-κB, as a key downstream transcription factor of TLR4, mediates the regulation of TLR4 on autophagy in UCM cardiomyocytes has not been clearly reported.

Based on these findings, we hypothesize that aberrant TLR4 activation in the uremic microenvironment regulates cardiomyocyte autophagy via NF-κB signaling, ultimately mediating myocardial injury and UCM progression. To test this hypothesis, a UCM rat model was established and treated with TLR4 inhibitor resatorvid (TAK-242) and NF-κB inhibitor JSH23. The role of the TLR4/NF-κB signaling pathway in regulating myocardial autophagy and pathological injury in UCM rats was systematically explored, aiming to elucidate the key molecular mechanisms underlying UCM and provide theoretical and experimental support for the development of targeted therapies.

Materials and Methods

Animal Ethics

Twenty-four 7-week-old male Sprague-Dawley rats (250 ± 20 g, Hangzhou Medical College, China) underwent a one-week adaptive feeding period in a specific pathogen-free (SPF) environment. The breeding conditions were controlled at 23 ± 1 ℃ with a 12-hour light-dark rhythm and *ad libitum* access to food and water. Upon approval from the Laboratory Animal Welfare Ethics Committee of Zhejiang Laboratory Animal Center (ZJCLA-IACUC-20011454), all procedures were performed strictly in compliance with relevant ethical standards and ARRIVE Guidelines 2.0.

Establishment of the UCM Model and Grouping

Male Sprague-Dawley rats (250 ± 20 g) were given a one-stage 5/6 nephrectomy to induce uraemia, as previously reported [17]. In brief, rats were anesthetized with isoflurane (3% for induction, then 2.5% for maintenance; 792632, Sigma-Aldrich, St. Louis, MO, USA). A laparotomy was then carried out, the left kidney was exposed, and approximately two-thirds of the kidney was resected, followed by the extraction of the right kidney. Care was taken to avoid injury to the adrenal glands. A sham procedure, including the decapsulation and intact replacement of both kidneys, was carried out for control animals.

All rats were randomly numbered by body weight using a random number table prior to surgery for randomization; grouping and subsequent sample testing were performed by independent researchers in a blinded manner. Rats were grouped into control, UCM, UCM + TAK-242, and UCM + JSH23. After the model establishment, in the UCM + TAK-242 group and the UCM + JSH23 group, rats were subcutaneously injected with 2 mg/kg/d of the TLR4 inhibitor TAK-242 (HY-11109, MCE, Princeton, NJ, USA) or 3 mg/kg/d of the NF-κB inhibitor JSH23 (HY-13982, MCE, Princeton, NJ, USA) for 4 weeks, and samples were collected 10 weeks later [18,19]. Animals with severe operative bleeding, adrenal injury, sustained poor mental status or death within the 10-week observation period were excluded from the study.

Transthoracic echocardiography was used to assess cardiac structure and function at weeks 4 and 10. In the tenth week, the rats were anesthetized with isoflurane (3% for induction, then 2.5% for maintenance). The depth of anesthesia was confirmed by the absence of pedal withdrawal and corneal reflexes. After confirmation of deep anesthesia, blood samples were collected from the abdominal aorta for subsequent serum analyses. Next, the rats were euthanized by cervical dislocation. To ensure the animals were completely unconscious and did not experience any distress, cervical dislocation was performed while the rats were still under deep anesthesia, confirmed by the lack of response to a firm toe pinch. Then, the heart was dissected to obtain a left ventricle sample for protein and histological analysis. Hematoxylin-eosin (HE) staining and Picro-sirius red/fast green staining (PSFG) sections were used to assess the cross-sectional area in order to confirm the development of left ventricular hypertrophy and fibrosis. Cell apoptosis was detected using Terminal Deoxynucleotidyl Transferase-Mediated dUTP Nick End Labeling (TUNEL). Immunofluorescence/Western blot analysis was used to evaluate protein expression associated with autophagy or TLR4/NF-κB signaling pathways.

Measurement of Creatinine and Urea Levels in Serum

Following blood serum sampling, the procedures were performed according to the manufacturer's instructions of the corresponding biochemical test kits for creatinine (S0291S, Beyotime, Shanghai, China) and urea (S0574M, Beyotime, Shanghai, China). First, the serum samples and standards were prepared and incubated with the reagents in the kits in proportion. Then, the reaction mixtures were incubated under the specified temperature for a certain period to complete the assay. After the reaction was completed, the absorbance values of each well were measured using an enzyme detector (Varioskan LUX, Thermo Fisher Scientific, Waltham, MA, USA) at the wavelength 570/670 nm. A standard curve was generated using absorbance data of the standards, and the specific concentrations of creatinine

(μmol/L) and urea (mmol/L) in the serum were calculated by substituting the sample absorbance values [20].

Enzyme-Linked Immunosorbent Assay (ELISA)

Serum levels of inflammatory cytokines, interleukin-1β (IL-1β, PI303), tumor necrosis factor-α (TNF-α, PT516), and interleukin-6 (IL-6, PI328) were detected using ELISA kits (Beyotime, China). First, 100 μL of serum samples or standards was loaded into the pre-coated wells and incubated at 37 °C for 2 hours. The plate was then washed three times (5 minutes each), followed by the addition of 100 μL of biotinylated detection antibody and incubation at 37 °C for 1 hour. After three additional washes, 100 μL of HRP-conjugated streptavidin was added and incubated at 37 °C for 20 min. Following three washes, 100 μL of TMB substrate solution was added and incubated at 37 °C in the dark for 20 min. The reaction was terminated by adding 50 μL of stop solution. The absorbance (450 nm) measurement using a microplate reader, the actual concentration of each inflammatory cytokine in the serum samples was calculated according to the standard curve and calculation formula provided in the ELISA kit instructions.

Echocardiography Experimental Procedures

Prior to echocardiographic detection, rats were anesthetized with isoflurane, and animals were placed on a heating pad to maintain normal body temperature during the examination. Cardiac morphology and function were assessed via transthoracic echocardiography (Vivid Q, GE Healthcare, Milwaukee, WI, USA) at 4 and 10 weeks post-model establishment: left ventricular internal diameter at systole (LVIDs), left ventricular internal diameter at diastole (LVIDd), and left ventricular ejection fraction (LVEF) were determined via M-mode echocardiography in anesthetized rats using parasternal short-/long-axis views at the papillary muscle level, while Doppler tissue imaging of transmitral flow and mitral annular signals was performed to assess the E/E' ratio (a key indicator of left ventricular diastolic function (E = peak early mitral inflow velocity; E' = peak early mitral annular velocity)). All data were analyzed using EchoPAC software (GE Healthcare, Milwaukee, WI, USA) by a blinded investigator, with mean values of triplicate measurements for statistical analysis.

HE and PSFG Staining

Formalin-fixed (G2161, Solarbio, Beijing, China) paraffin-embedded (C06415103, Nanjing Reagent, Nanjing, China) subvalvular sections of the left ventricle were cut into 5 μm slices.

HE staining (C0105S, Beyotime, Shanghai, China): Sections were stained with HE reagents following standard protocols, dehydrated, and mounted. Blue-stained nuclei and pink-stained cytoplasm of cardiomyocytes were visualized to assess cellular morphology. Pathological changes of left ventricle tissues were finally observed under an optical microscope (400×, THUNDER Imager Tissue, Leica, Wetzlar, Germany).

PSFG staining: Sections were stained with picrosirius red (365548, Sigma Aldrich, St. Louis, MO, USA) (stains collagen red) and fast green (HY-D0914, MCE, Princeton, NJ, USA) (stains cardiac muscle green), dehydrated, and mounted. The cardiac fibrosis condition was observed under a 400× magnification microscope.

TUNEL Assay

Myocardial paraffin sections were dewaxed in xylene (C04305302, Nanjing Reagent, Nanjing, China) (two cycles, 5–10 min each), rehydrated in graded ethanol (C06915100, Nanjing Reagent, Nanjing, China), and rinsed in distilled water. Sections were digested (20 μg/mL proteinase K; ST532, Beyotime, Shanghai, China) (37 °C, 15 min) and blocked (3% hydrogen peroxide solution; 88597, Millipore, Bradford, MA, USA) (room temperature, 20 min). Following PBS washes, sections experienced cultivation with 50 μL TUNEL reaction mixture (G4891, Solarbio, Beijing, China) containing terminal deoxynucleotidyl transferase (TdT) and biotinylated dUTP (37 °C, 60 min), washing with PBS, and 30-min culture with Streptavidin-HRP solution (G4891, Solarbio, Beijing, China) (37 °C). Following washing with PBS, the sections were developed using 3,3′-Diaminobenzidine (DAB), counterstained with hematoxylin (HY-K0315, MCE, Princeton, NJ, USA), dehydrated, cleared, and mounted. Five random fields/sections were captured under a light microscope (200× magnification). The apoptotic level was quantified as the percentage of TUNEL-positive cells.

Western Blotting

For protein extraction, tissue and cell lysates were prepared in radioimmunoprecipitation assay buffer (RI-PA lysate; R0010, Solarbio, Beijing, China). Protein concentrations were determined using bicinchoninic acid assay (BCA; BCA1, Sigma-Aldrich, St. Louis, MO, USA). Following sodium dodecyl sulfate-polyacrylamide gel electrophoresis (SDS-PAGE; P0012A, Beyotime, Shanghai, China) fractionation, the separated proteins were wet transferred to a polyvinylidene fluoride membrane (YA1700, Solarbio, Beijing, China). Before adding the primary antibody dilution (Table 1), the membrane was blocked (1.5 hours, room temperature) using 5% skim milk. Secondary antibodies (Table 1) were incubated for two hours the next day, after primary antibodies were incubated at 4 °C overnight. Following band visualization with a gel imaging equipment (ChampGel®7800, SINSAGE, Beijing, China), grayscale analysis was performed employing ImageJ software (Version 1.52a, National Institutes of Health, Bethesda, MD, USA).

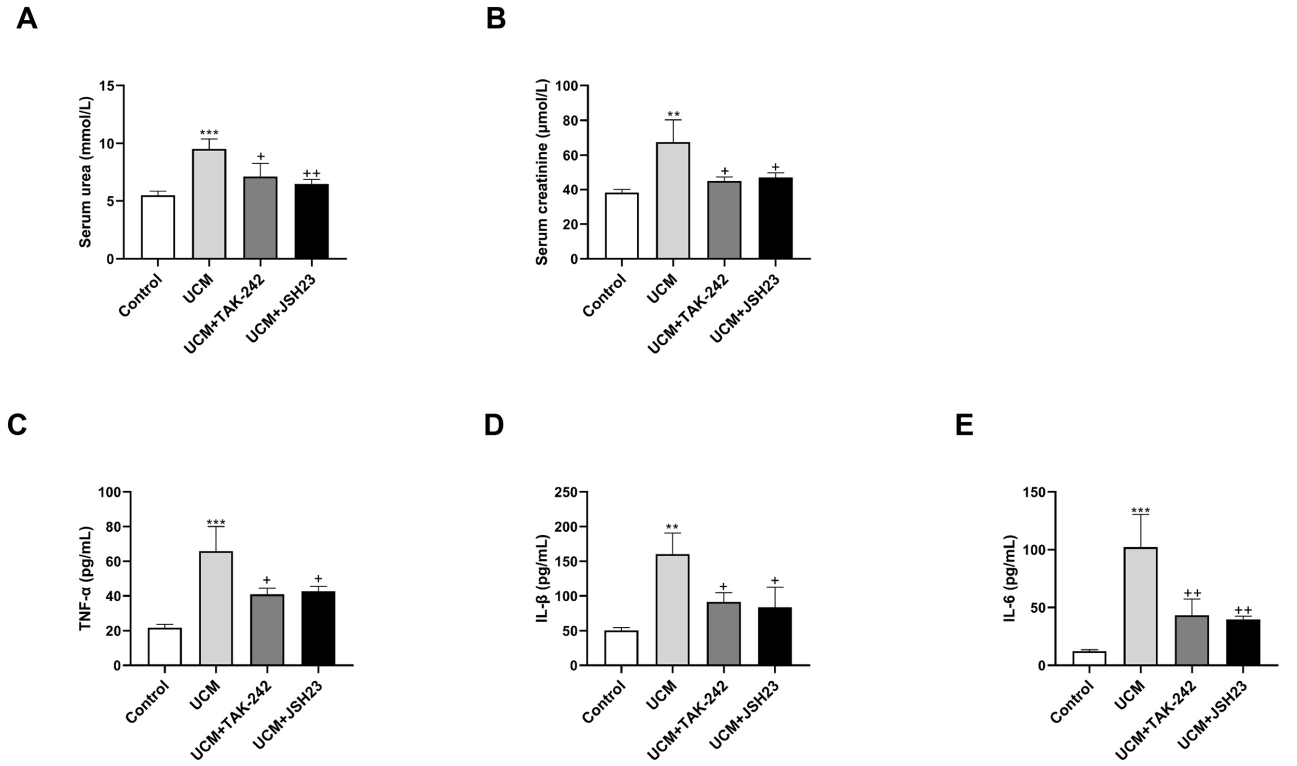

Fig. 1. Serum biochemical and inflammatory cytokine levels in rats with uraemic cardiomyopathy (UCM). (A) Serum urea levels, (B) serum creatinine levels, (C) tumor necrosis factor-α (TNF-α) levels, (D) interleukin-1β (IL-1β) levels, and (E) interleukin-6 (IL-6) levels in the Control, UCM, UCM+Resatorvid (TAK-242, TLR4 inhibitor), and UCM+JSH23 (NF-κB inhibitor) groups. Serum parameters were detected using enzyme-linked immunosorbent assay (ELISA) kits. Data are presented as mean ± SD (n = 6 rats/group). $^{**}p < 0.01$, $^{***}p < 0.001$ vs. Control; $^{+}p < 0.05$, $^{++}p < 0.01$ vs. UCM. NF-κB, nuclear factor kappa-B.

Table 1. Antibodies used in this study.

Name	Catalog	Molecular weight (kDa)	Dilution	Manufacturer
TLR4	sc-293072	95	1/1000	Santacruz, CA, USA
MyD88	ab219413	33	1/1000	abcam, Cambridge, UK
p-P65	#3033	65	1/1000	Cell Signaling Technology, Danvers, MA, USA
P65	#8242	65	1/1000	Cell Signaling Technology, Danvers, MA, USA
LC3B	ab192890	14/16	1/2000	abcam, Cambridge, UK
Beclin1	ab207612	52	1/1000	abcam, Cambridge, UK
GAPDH	ab8245	36	1/10,000	abcam, Cambridge, UK
Goat anti-mouse	ab205719	—	1/2000	abcam, Cambridge, UK
Goat anti-rabbit	ab205718	—	1/2000	abcam, Cambridge, UK

TLR4, toll-like receptor 4; MyD88, myeloid differentiation factor 88; LC3B, microtubule-associated protein 1 light chain 3 beta; GAPDH, glyceraldehyde-3-phosphate dehydrogenase.

Immunofluorescence

Myocardial paraffin sections experienced dewaxing, rehydration and antigen retrieval. After blocking nonspecific binding, sections were incubated with primary antibody Phospho-NF-κB p65 (p-P65; #AF2006, Affinity Biosciences, Jiangsu, China) (overnight at 4 °C), followed by incubation with fluorescently labeled secondary antibody (A-11008, Thermo Fisher Scientific, Waltham, MA, USA). Nuclei were counterstained with 4′,6-Diamidino-2-phenylindole (DAPI, C0065, Solarbio, Beijing, China). Images were captured under a fluorescence microscope (×200 magnification), with DAPI staining (blue) marking cell nuclei and green fluorescence representing p-P65 protein expression. The staining intensity of p-P65 was quantitatively analyzed based on the collected immunofluorescence images to quantify p-P65 protein in myocardial tissues.

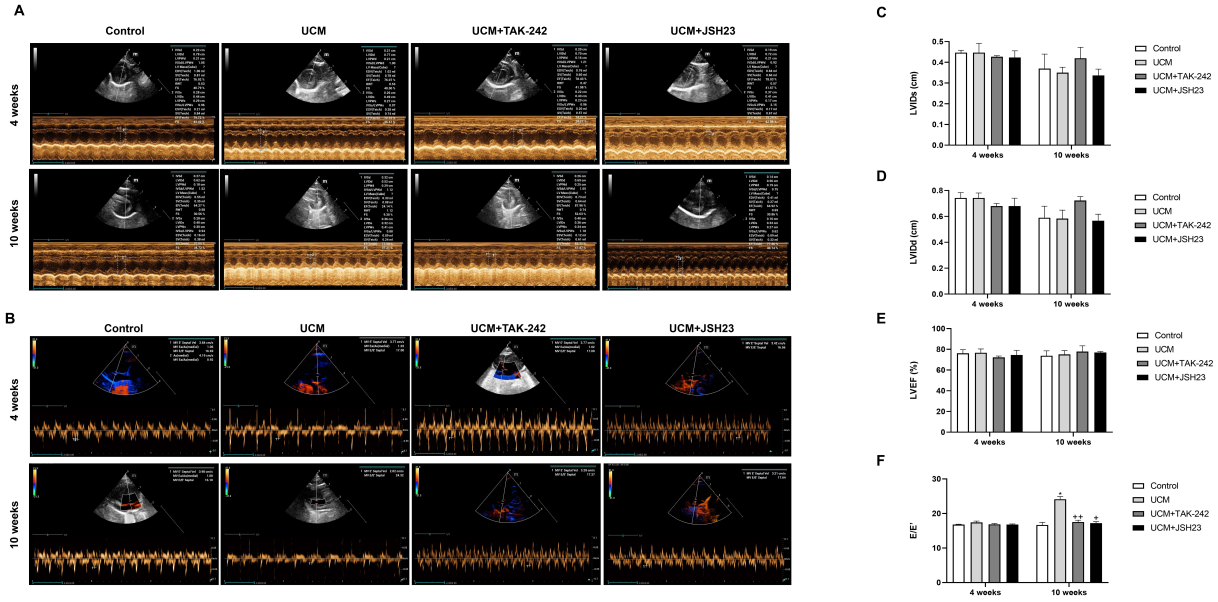

Fig. 2. Cardiac structure and function assessment in rats with UCM via transthoracic echocardiography. (A) M-mode echocardiographic images, (B) Doppler tissue imaging (DTI) images, (C) left ventricular internal diameter at systole (LVIDs), (D) left ventricular internal diameter at diastole (LVIDd), (E) left ventricular ejection fraction (LVEF), and (F) E/E' ratio (a key indicator of left ventricular diastolic function (E = peak early mitral inflow velocity; E' = peak early mitral annular velocity)) in the Control, UCM, UCM+TAK-242, and UCM+JSH23 groups at weeks 4 and 10. Echocardiographic parameters were analyzed using EchoPAC software. Data are presented as mean ± SD (n = 6 rats/group). $^{*}p < 0.05$ vs. Control; $^{+}p < 0.05$, $^{++}p < 0.01$ vs. UCM.

Statistical Analysis

GraphPad Prism 8.0 (GraphPad Prism Software, San Diego, CA, USA) was used for statistical analysis [21]. The mean ± standard deviation was used to express the measurement data. One-way analysis of variance (ANOVA) or repeated measures ANOVA was employed for comparisons among multiple groups, followed by Tukey's post-hoc test for pairwise comparisons. $p < 0.05$ was indicative of statistical significance.

Results

TLR4 and NF-κB Inhibition Reverse the Increase in Urea, Creatinine and Inflammatory Factor Levels in UCM Rats

To elucidate the role of the TLR4 and NF-κB in UCM, we analyzed serum biochemical and inflammatory cytokine levels across experimental groups. As shown in Fig. 1A,B, serum urea and creatinine levels were higher in the UCM group than in the Control group ($P < 0.01$), confirming the successful establishment of uraemia. Notably, administration of TAK-242 (TLR4 inhibitor) or JSH23 (NF-κB inhibitor) significantly reduced both urea and creatinine levels (Fig. 1A,B, $p < 0.05$), indicating attenuation of renal dysfunction in UCM rats. For inflammatory responses, the results demonstrated significantly increased serum levels of TNF-α, IL-1β, and IL-6 in the UCM group (Fig. 1C–E, $p < 0.01$ vs. Control). Treatment with TAK-242 or JSH23 notably downregulated these pro-inflammatory cytokines (Fig. 1C–E, $p < 0.05$), suggesting that TLR4/NF-κB signaling drives systemic inflammation in UCM.

TLR4 and NF-κB Inhibition Limits the UCM Echocardiographic Signs

To unveil the role of the TLR4/NF-κB signaling pathway in cardiac structure and function of rats with UCM, transthoracic echocardiography was performed at weeks 4 and 10. The UCM group showed a downward trend in the systolic LVIDs and diastolic LVIDd at week 10 (Fig. 2A,C,D). In contrast, the LVIDs and LVIDd of rats treated with TAK-242 showed an upward trend at the 10th week (Fig. 2A,C,D). Overall, LVIDs and LVIDd did not differ significantly among the groups (Fig. 2A,C,D).

For the contraction function, as shown in Fig. 2E, LVEF was comparable among all groups at weeks 4 and 10. In contrast, the left ventricular mitral valve blood flow pattern in the UCM group was abnormal (Fig. 2B,F), while TAK-242 and JSH23 treatments partially restored diastolic function. At the 10th week, the E/E' ratio was significantly reduced in the TAK-242 and JSH23 treatment groups (Fig. 2F, $p < 0.05$).

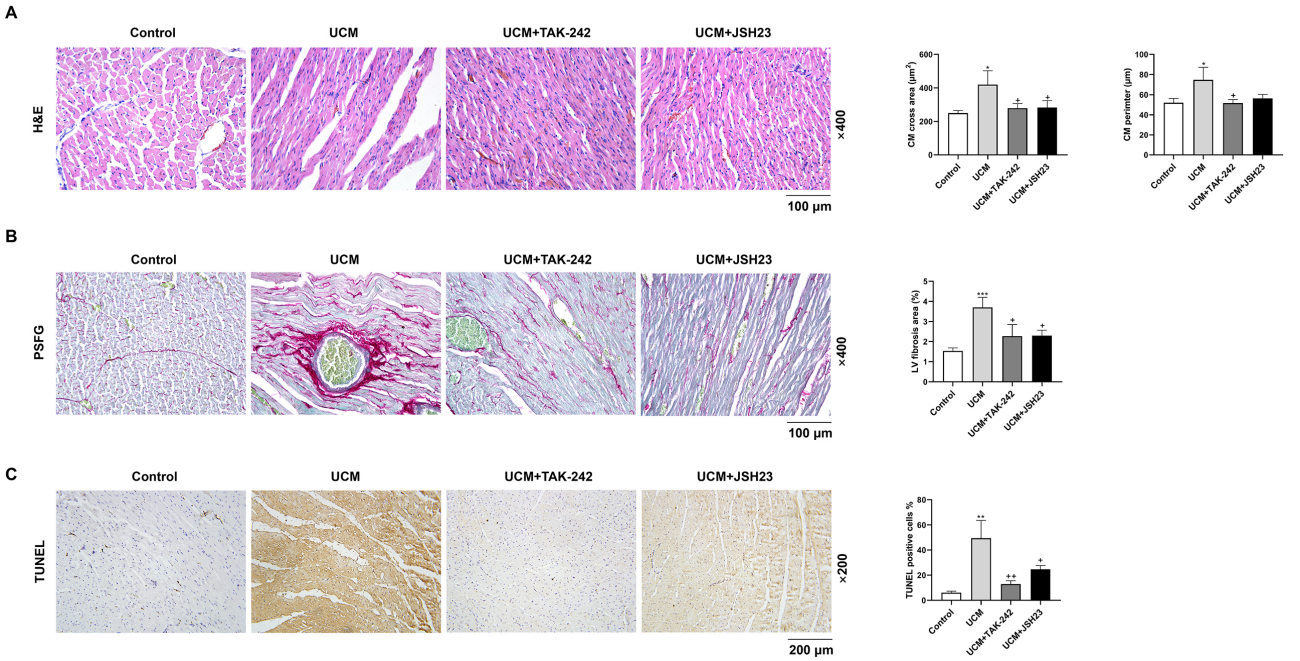

Fig. 3. Histopathological and apoptotic changes in myocardial tissues of rats with UCM. (A) Cardiomyocyte morphology and arrangement (blue-stained nuclei, pink-stained cytoplasm) (Hematoxylin-eosin (HE) staining; ×400, scale bar: 100 μm). Bar graphs on the right show quantitative analysis of cardiomyocyte (CM) cross-sectional area (μm^2) and perimeter (μm). (B) Collagen fibers (red) and cardiac muscle (green) (Picro-sirius red and fast green (PSFG) staining; ×400, bar: 100 μm). The bar graph illustrates the percentage of left ventricular (LV) fibrosis area (%). (C) Apoptotic cells in the Control, UCM, UCM+TAK-242, and UCM+JSH23 groups (Terminal deoxynucleotidyl transferase-mediated dUTP nick end labeling (TUNEL) staining; ×200, bar: 200 μm). The bar graph displays the percentage of TUNEL-positive cells (%). Data are presented as mean ± SD (n = 6 rats/group). $^{*}p < 0.05$, $^{**}p < 0.01$, $^{***}p < 0.001$ vs. Control; $^{+}p < 0.05$, $^{++}p < 0.01$ vs. UCM.

TLR4 and NF-κB Inhibition Alleviates Myocardial Injury in UCM

To elucidate the influence of TLR4/NF-κB signaling in myocardial histopathological alterations of UCM, we performed histological staining and apoptosis detection. As shown in Fig. 3A (HE staining), the control group exhibited an orderly cardiomyocyte (CM) arrangement with normal cellular morphology. In contrast, the UCM group showed marked cardiomyocyte hypertrophy and disorganized arrangement, with significantly increased CM cross-sectional area and perimeter (Fig. 3A, $p < 0.05$). Notably, TAK-242 treatment significantly alleviated these hypertrophic changes, JSH23 significantly reduced only the CM cross-sectional area ($p < 0.05$ vs. UCM group), with cardiomyocytes appearing more organized and closer to normal morphology (Fig. 3A).

Cardiac fibrosis was assessed by PSFG staining. In the control group, collagen fibers (stained red) were sparsely distributed in the myocardium (Fig. 3B). In contrast, the UCM group exhibited extensive collagen deposition, particularly in the perivascular and interstitial regions, accompanied by a significant increase in the left ventricular (LV) fibrotic area (Fig. 3B, $p < 0.001$). Treatment with either TAK-242 or JSH23 significantly attenuated collagen accumulation, indicating a reduction in fibrotic progression (Fig. 3B, $p < 0.05$).

TUNEL staining (Fig. 3C) was used to evaluate cardiomyocyte apoptosis, and the nuclei of apoptotic cells were brown to brownish-black. Few TUNEL-positive cells were observed in the control group, whereas the number of TUNEL-positive cells was markedly elevated in the UCM group, confirming enhanced cardiomyocyte apoptosis in UCM myocardial tissues (Fig. 3C, $p < 0.01$). Notably, TAK-242 and JSH23 interventions significantly reduced TUNEL-positive cells, suggesting that both agents could effectively suppress myocardial apoptosis (Fig. 3C, $p < 0.05$).

TLR4 and NF-κB Inhibition Restricts UCM Autophagy and the TLR4/NF-κB Signaling Pathway

For autophagic activity, Fig. 4A–C shows upregulated LC3II/I (a marker of autophagosome formation) and Beclin 1 (a key autophagy initiator) ($p < 0.001$) in the UCM group. Treatment with TAK-242 or JSH23 notably reduced LC3II/I and Beclin 1 expression (Fig. 4A–C, $p < 0.05$). This suggests that TLR4/NF-κB signaling impacts autophagy-related protein expression in the setting of UCM. For the TLR4/NF-κB signaling cascade, Fig. 4D–G demonstrates that TLR4, myeloid differentiation factor 88

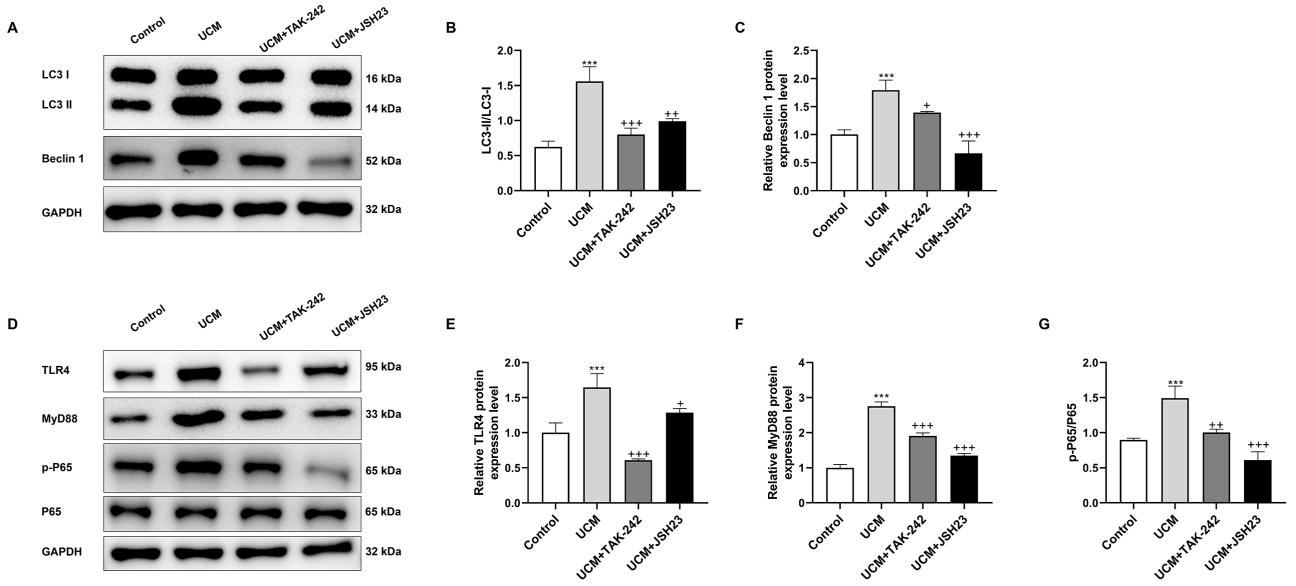

Fig. 4. Protein expression of autophagy-related and toll-like receptor 4 (TLR4)/nuclear factor kappa-B (NF-κB) signaling molecules in myocardial tissues of rats with UCM. (A) Microtubule-associated protein 1 light chain 3 (LC3 I, LC3 II), Beclin 1, and glyceraldehyde-3-phosphate dehydrogenase (GAPDH; a loading control) (Western blotting). (B) LC3II/LC3I ratio. (C) Beclin 1 protein expression. (D) TLR4, myeloid differentiation factor 88 (MyD88), phosphorylated-RelA (p-P65), P65, and GAPDH (Western blotting). (E) TLR4 protein expression. (F) MyD88 protein expression. (G) p-P65/P65 ratio. Data are presented as mean ± SD (n = 6 rats/group). $^{***}p < 0.001$ vs. Control; $^{+}p < 0.05$, $^{++}p < 0.01$, $^{+++}p < 0.001$ vs. UCM.

(MyD88) (an adaptor protein in TLR4 signaling), and phosphorylated P65 (p-P65, an activated form of NF-κB)/P65 ratio were significantly upregulated in the UCM group ($p <$ 0.001 vs. control). Treatment of TAK-242 or JSH23 effectively downregulated TLR4, MyD88, and p-P65/P65 (Fig. 4D–G, $p < 0.05$).

Both TLR4 and NF-κB Inhibit the Fluorescence Intensity of p-P65

To assess the activation status of NF-κB signaling in myocardium during UCM, immunofluorescence staining for p-P65 was performed. p-P65 fluorescence intensity (green) was low in the control group (Fig. 5). In contrast, the UCM group exhibited a marked increase in p-P65 fluorescence intensity, indicating robust activation of NF-κB signaling (Fig. 5, $p < 0.001$). Treatment with TAK-242/JSH23 significantly reduced p-P65 fluorescence intensity (Fig. 5, $p < 0.01$). Accordingly, these findings suggest activation of the TLR4/NF-κB signaling pathway in UCM myocardium.

Discussion

UCM is a fatal complication for CKD patients, and its pathological mechanism involves the complex interaction of inflammatory storm, myocardial remodeling and metabolic disorder [22]. Currently, the synergistic effect of TLR4-mediated inflammatory signaling and autophagy dysregulation remains a research focus [23]. Although there are few studies on TLR4 in UCM, Hui et al. found that TLR4 and MyD88 were upregulated in diabetic cardiomyopathy and closely associated with cardiomyocyte apoptosis [24]. Consistently, we revealed increased expression of TLR4 and its downstream MyD88 proteins in UCM model rats, confirming the key role of TLR4 signaling in UCM. Importantly, this study further revealed the mediating role of autophagy in this process.

Abnormally activated TLR4/NF-κB pathway is a common pathological basis for various types of cardiomyopathy [25]. Zhao et al. [26] revealed that the TLR4 inhibitor TAK-242 alleviated diabetic cardiomyopathy by inhibiting pyroptosis and the TLR4/calcium/calmodulin-dependent protein kinase II (CaMKII)/NLRP3 pathway. In this study, treatment with TAK-242 and JSH23 decreased the levels of TNF-α and IL-1β in the serum of UCM rats and reduced the degree of myocardial fibrosis, which corresponds to the reported mechanisms in other disease models. As the core indicator of autophagic activity, the LC3II/I ratio directly reflects the efficiency of autophagosome formation. Beclin 1 is the key molecule regulating the initiation of autophagy. Together, these markers provide an important reference for evaluating autophagy-related molecular changes [27]. Notably, the present study provides new evidence for the association between the TLR4/NF-κB pathway and autophagy in UCM. In the UCM model group, both the LC3II/I ratio and Beclin 1 expression were significantly increased, whereas treatment with TLR4/NF-

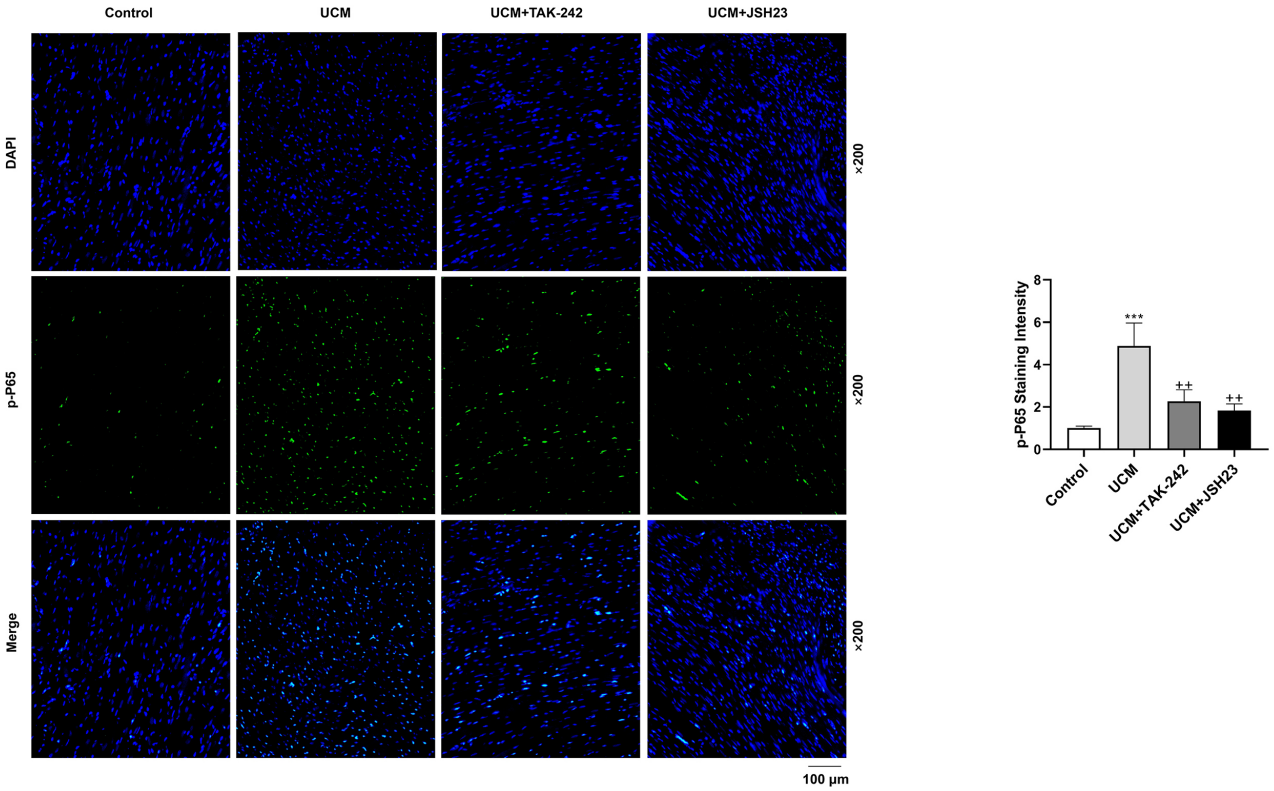

Fig. 5. Immunofluorescence analysis of p-P65 in myocardial tissues of rats with UCM. 4′,6-diamidino-2-phenylindole (DAPI, blue) for nuclear staining and p-P65 (green) expression in myocardial tissues of the Control, UCM, UCM+TAK-242, and UCM+JSH23 groups (Immunofluorescence; ×200, bar: 100 μm). Data are presented as mean ± SD (n = 6 rats/group). $^{***}p < 0.001$ vs. Control; $^{++}p < 0.01$ vs. UCM.

κB inhibitors downregulated these autophagy-related markers. These findings suggest that the TLR4/NF-κB signaling axis may participate in UCM progression by modulating autophagy-associated protein expression, providing a novel mechanistic perspective on "inflammation-autophagy" to the TLR4-mediated myocardial injury.

Autophagy exerts bidirectional modulatory effects during the occurrence and progression of various cardiomyopathic diseases. Moderate physiological autophagy eliminates impaired organelles and abnormal proteins, thereby relieving myocardial oxidative stress and tissue injury. In contrast, persistent upregulation of autophagy-related molecules disrupts cellular homeostasis and facilitates cardiomyocyte apoptosis [28,29]. As a well-established key indicator of NF-κB pathway activation, p-P65 expression level directly and objectively reflects the overall activation status of NF-κB signaling [30]. In our study, myocardial p-P65 expression was markedly upregulated in UCM rats, which was consistent with the altered trends of LC3II/I ratio and Beclin 1 expression. These results confirm a close correlation between elevated NF-κB signaling activity and abnormal changes in autophagy-associated molecules during uremic myocardial damage.

The present study has several limitations. First, all mechanistic investigations were performed solely using animal models, without further validation in clinical specimens. In addition, our evaluation of autophagy only relied on detecting the LC3II/I ratio and Beclin 1 expression. These two biomarkers merely reflect autophagosome biogenesis and fail to differentiate elevated autophagic flux from autophagosome accumulation caused by blocked degradation. Further studies incorporating p62 detection and transmission electron microscopy are needed to comprehensively evaluate the actual status of autophagic flux in UCM.

Conclusions

In conclusion, this study verified that the TLR4/NF-κB signaling axis modulates the expression of autophagy-associated proteins and triggers abnormal alterations in autophagy-related molecular profiles, thereby accelerating the pathological progression of UCM. Future research can focus on the expression characteristics of the molecules in this pathway in clinical samples, combine single-cell sequencing technology to analyze the activation differences of the pathway in different cell types, and develop dual-target inhibitors of TLR4/NF-κB that can penetrate myocar-

dial tissue, providing a more robust experimental basis and transformation direction for the precise treatment of UCM.

Availability of Data and Materials

The analyzed datasets generated during the study are available from the corresponding author on reasonable request.

Author Contributions

HPZ and WNW designed the research study; LTP performed the research; ZYD and SSC collected and analyzed the data. SSC has been involved in drafting the manuscript and all authors have been involved in revising it critically for important intellectual content. All authors gave final approval of the version to be published. All authors have participated sufficiently in the work to take public responsibility for appropriate portions of the content and agreed to be accountable for all aspects of the work in ensuring that questions related to its accuracy or integrity.

Ethics Approval and Consent to Participate

This animal experiment was approved by the Laboratory Animal Welfare Ethics Committee of Zhejiang Laboratory Animal Center (ZJCLA-IACUC-20011454), and all procedures were performed in strict compliance with relevant ethical standards and ARRIVE Guidelines 2.0.

Acknowledgment

Not applicable.

Funding

This study was supported by Zhejiang Provincial Health Commission, Zhejiang Provincial Medical and Health Science and Technology Plan Project (Grant number 2023RC112).

Conflict of Interest

The authors declare no conflict of interest.

References

[1] Jankowski J, Floege J, Fliser D, Böhm M, Marx N. Cardiovascular Disease in Chronic Kidney Disease: Pathophysiological Insights and Therapeutic Options. Circulation. 2021; 143: 1157–1172. https://doi.org/10.1161/CIRCULATIONAHA.120.050686

[2] Marx-Schütt K, Cherney DZI, Jankowski J, Matsushita K, Nardone M, Marx N. Cardiovascular disease in chronic kidney disease. European Heart Journal. 2025; 46: 2148–2160. https://doi.org/10.1093/eurheartj/ehaf167

[3] Song Q, Wang P, Wu Y, Yao Z, Wang W, Tang G, et al. Understanding uremic cardiomyopathy: from pathogenesis to diagnosis and the horizon of therapeutic innovations. PeerJ. 2025; 13: e18978. https://doi.org/10.7717/peerj.18978

[4] Dalpathadu H, Salim AM, Wade A, Greenway SC. A Systematic Review of Uremic Toxin Concentrations and Cardiovascular Risk Markers in Pediatric Chronic Kidney Disease. Toxins. 2024; 16: 345. https://doi.org/10.3390/toxins16080345

[5] Nguyen TD, Schulze PC. Cardiac Metabolism in Heart Failure and Implications for Uremic Cardiomyopathy. Circulation Research. 2023; 132: 1034–1049. https://doi.org/10.1161/CIRCRESAHA.123.321759

[6] Arcari L, Camastra G, Ciolina F, Danti M, Cacciotti L. T_1 and T_2 Mapping in Uremic Cardiomyopathy: An Update. Cardiac Failure Review. 2022; 8: e02. https://doi.org/10.15420/cfr.2021.19

[7] Curaj A, Vanholder R, Loscalzo J, Quach K, Wu Z, Jankowski V, et al. Cardiovascular Consequences of Uremic Metabolites: an Overview of the Involved Signaling Pathways. Circulation Research. 2024; 134: 592–613. https://doi.org/10.1161/CIRCRESAHA.123.324001

[8] Esposito P, Verzola D, Saio M, Picciotto D, Frascio M, Laudon A, et al. The Contribution of Muscle Innate Immunity to Uremic Cachexia. Nutrients. 2023; 15: 2832. https://doi.org/10.3390/nu15132832

[9] Sun C, Li W, Li Y, Chen J, An H, Zeng G, et al. MiR-182-5p Mediated by Exosomes Derived From Bone Marrow Mesenchymal Stem Cell Attenuates Inflammatory Responses by Targeting TLR4 in a Mouse Model of Myocardial Infraction. Immune Network. 2022; 22: e49. https://doi.org/10.4110/in.2022.22.e49

[10] Ma Z, Li X, Fan RLY, Yang KY, Ng CSH, Lau RWH, et al. A human pluripotent stem cell-based model of SARS-CoV-2 infection reveals an ACE2-independent inflammatory activation of vascular endothelial cells through TLR4. Stem Cell Reports. 2022; 17: 538–555. https://doi.org/10.1016/j.stemcr.2022.01.015

[11] Fu Y, Gong T, Loughran PA, Li Y, Billiar TR, Liu Y, et al. Roles of TLR4 in macrophage immunity and macrophage-pulmonary vascular/lymphatic endothelial cell interactions in sepsis. Communications Biology. 2025; 8: 469. https://doi.org/10.1038/s42003-025-07921-3

[12] Du J, Liu Y, Fu J. Autophagy, Myocarditis, and Cardiomyopathy. Advances in Experimental Medicine and Biology. 2020; 1207: 229–235. https://doi.org/10.1007/978-981-15-4272-5_17

[13] Singh SR, Zech ATL, Geertz B, Reischmann-Düsener S, Osinska H, Prondzynski M, et al. Activation of Autophagy Ameliorates Cardiomyopathy in *Mybpc3*-Targeted Knockin Mice. Circulation. Heart Failure. 2017; 10: e004140. https://doi.org/10.1161/CIRCHEARTFAILURE.117.004140

[14] Feng J, Li H, Wang S. Hydrogen sulfide alleviates uremic cardiomyopathy by regulating PI3K/PKB/mTOR-mediated overactive autophagy in 5/6 nephrectomy mice. Frontiers in Pharmacology. 2022; 13: 1027597. https://doi.org/10.3389/fphar.2022.1027597

[15] Wang S, Zhang K, Song X, Huang Q, Lin S, Deng S, et al. TLR4 Overexpression Aggravates Bacterial Lipopolysaccharide-Induced Apoptosis via Excessive Autophagy and NF-κB/MAPK Signaling in Transgenic Mammal Models. Cells. 2023; 12: 1769. https://doi.org/10.3390/cells12131769

[16] Zhang Q, Wang L, Wang S, Cheng H, Xu L, Pei G, et al. Signaling pathways and targeted therapy for myocardial infarction. Signal Transduction and Targeted Therapy. 2022; 7: 78. https://doi.org/10.1038/s41392-022-00925-z

[17] Taylor D, Bhandari S, Seymour AML. Mitochondrial dysfunction in uremic cardiomyopathy. American Journal of Physiology. Renal Physiology. 2015; 308: F579–F587. https://doi.org/10.1152/ajprenal.00442.2014

[18] Zhang Y, Peng W, Ao X, Dai H, Yuan L, Huang X, et al. TAK-242, a Toll-Like Receptor 4 Antagonist, Protects against

Aldosterone-Induced Cardiac and Renal Injury. PloS One. 2015; 10: e0142456. https://doi.org/10.1371/journal.pone.0142456

[19] Nassar A, Kaplanski J, Azab AN. A Selective Nuclear Factor-κB Inhibitor, JSH-23, Exhibits Antidepressant-like Effects and Reduces Brain Inflammation in Rats. Pharmaceuticals (Basel, Switzerland). 2024; 17: 1271. https://doi.org/10.3390/ph17101271

[20] Hu H, Guo Y, Zhang L, Li K. The Protective Effects and Mechanism of Mulberry Leaf Flavonoids on Type 2 Diabetic Nephropathy Mice. Journal of Experimental and Clinical Application of Chinese Medicine. 2024; 5: 56–68. https://doi.org/10.62767/jecacm504.7832

[21] Huang F, He K. Rhizoma Zedoariae Inhibits G-CSF-Induced MDSCs-like Differentiation of THP-1 Cells. Journal of Experimental and Clinical Application of Chinese Medicine. 2024; 5: 12-22.

[22] Markwirth P, Selejan SR, Hohl M, Schunk SJ, Müller A, Wagenpfeil S, et al. Renal Denervation Improves Uremic Cardiomyopathy in Rats With Chronic Kidney Disease. Journal of the American Heart Association. 2025; 14: e038785. https://doi.org/10.1161/JAHA.124.038785

[23] Qin Y, Li K, Zhang Q, Liu J, Xie Y, Zhang T, et al. Linoleic acid inhibits lipopolysaccharide-induced inflammation by promoting TLR4 regulated autophagy in murine RAW264.7 macrophages. Journal of Applied Biomedicine. 2024; 22: 185–196. https://doi.org/10.32725/jab.2024.023

[24] Shi H, Zhou P, Ni YQ, Wang SS, Song R, Shen AL, et al. *In vivo and in vitro* studies of Danzhi Jiangtang capsules against diabetic cardiomyopathy via TLR4/MyD88/NF-κB signaling pathway. Saudi Pharmaceutical Journal : SPJ : the Official Publication of the Saudi Pharmaceutical Society. 2021; 29: 1432–1440. https://doi.org/10.1016/j.jsps.2021.11.004

[25] Zhou X, Xing S, Zhang L, Lu J, Li D, Wang Y, et al. Amniotic mesenchymal stem cells attenuate diabetic cardiomyopathy by inhibiting pyroptosis via modulation of the TLR4/NF-κb/NLRP3 pathway. Frontiers in Cell and Developmental Biology. 2025; 13: 1631973. https://doi.org/10.3389/fcell.2025.1631973

[26] Zhao X, Zhang J, Xu F, Shang L, Liu Q, Shen C. TAK-242 alleviates diabetic cardiomyopathy via inhibiting pyroptosis and TLR4/CaMKII/NLRP3 pathway. Open Life Sciences. 2024; 19: 20220957. https://doi.org/10.1515/biol-2022-0957

[27] Eid N, Davamani F. Human β-defensin-1 activates autophagy in human colon cancer cells *via* regulation of long non-coding RNA TCONS_00014506. World Journal of Gastrointestinal Oncology. 2024; 16: 2894–2901. https://doi.org/10.4251/wjgo.v16.i7.2894

[28] Wang H, Wang L, Hu F, Wang P, Xie Y, Li F, et al. Neuregulin-4 attenuates diabetic cardiomyopathy by regulating autophagy via the AMPK/mTOR signalling pathway. Cardiovascular Diabetology. 2022; 21: 205. https://doi.org/10.1186/s12933-022-01643-0

[29] Liu D, Xing R, Zhang Q, Tian X, Qi Y, Song H, et al. The CREG1-FBXO27-LAMP2 axis alleviates diabetic cardiomyopathy by promoting autophagy in cardiomyocytes. Experimental & Molecular Medicine. 2023; 55: 2025–2038. https://doi.org/10.1038/s12276-023-01081-2

[30] Feng W, Niu N, Lu P, Chen Z, Rao H, Zhang W, et al. Multilevel Regulation of NF-κB Signaling by NSD2 Suppresses Kras-Driven Pancreatic Tumorigenesis. Advanced Science (Weinheim, Baden-Wurttemberg, Germany). 2024; 11: e2309387. https://doi.org/10.1002/advs.202309387